Mathematical Biology

Antigen receptor therapy in bone metastasis via optimal control for different human life stages

Silvia Jerez[1] · **Emilene Pliego[1]** · **Francisco J. Solis[1]** · **Anna K. Miller[2]**

Abstract

In this work we propose a bone metastasis model using power law growth functions in order to describe the biochemical interactions between bone cells and cancer cells. Experimental studies indicate that bone remodeling cycles are different for human life stages: childhood, young adulthood, and adulthood. In order to include such differences in our study, we estimate the model parameter values for each human life stage via bifurcation analysis. Results reveal an intrinsic relationship between the active period of remodeling cycles and the proliferation of cancer cells. Subsequently, using optimal control theory we analyze a possible antigen receptor therapy as a new treatment for bone metastasis. Theoretical results such as existence of optimal solutions are proved. Numerical simulations for late stages of bone metastasis are presented and a discussion of our results is carried out.

✉ Silvia Jerez
   jerez@cimat.mx

   Emilene Pliego
   emilene.pliego@cimat.mx

   Francisco J. Solis
   solis@cimat.mx

   Anna K. Miller
   anna.miller@moffitt.org

[1] CIMAT, 36000 Guanajuato, Gto, Mexico

[2] Moffitt Cancer Center, 12902 USF Magnolia Drive, Tampa, FL, USA

⚛ Springer

1 Introduction

Several kinds of tumors can grow in bones like a primary cancer, some examples are multiple myeloma, osteosarcoma, lymphoma, etc. However, a metastasis bone cancer takes place in the late-stage of different types of tumors like breast, prostate and lung cancers, when tumor cells travel through the blood from their primary location to some place of the skeleton (Randall et al. 2016). Bone metastasis depends on the properties and characteristics of tumor cells and the bone cellular microenvironment. There are two relevant cell populations involved in the bone microenvironment: osteoclast cells and osteoblast cells. These cells are in charge of the bone remodeling process and also are an essential part of a *basic multicellular unit* (BMU). Osteoclasts resorb bone in response to signals which are related to bone damage and next, with the release of biochemical growth factors, osteoblasts start the bone formation (Jilka 2003; Bilezikian et al. 2008). When cancer cells are present in the bone microenvironment, they release several regulatory factors that result in abnormal bone destruction and/or formation. This can result in osteolytic or osteoblastic lesions, respectively. In particular, destruction of the mineralized matrix is necessary for the metastatic proliferation (Randall et al. 2016). This complex interplay between cancer cells and bone cells establishes a feed-forward *vicious cycle*[1] that leads to a selective growth advantage for cancer cells (Paget 1889; Mundy 2002). Significant progress has been made in the study of bone metastasis Biology. Jinnah et al. (2018) offer an overview of the in vivo models, keeping abreast of advances and efforts to treat bone metastases and to understand the progression, cellular players, and signaling pathways driving bone metastasis.

To mathematically model the complex interaction between BMU cells and cancer cells requires a representation general enough to capture the essence of the observed response that, at the same time, is mathematically manageable. One approach that satisfies these requirements is the power-law formalism proposed to capture the essential autocrine and paracrine signalling of complex biochemical processes (Savageau 1988; Voit 1991). Based on such approach a family of biochemical simplified models, initially derived by Komarova et al. (2003), has been proposed that describes temporal changes in osteoclast cells and osteoblast cells (Ryser et al. 2010; Zumsande et al. 2011; Jerez and Chen 2015; Garzón-Alvarado 2012). In such direction, some authors have used this biochemical-simplified formulation to model the interactions between bone cells and cancer cells and have obtained significant insights about proliferation or eradication of cancer cells (Ayati et al. 2010; Koenders and Saso 2016; Jerez and Camacho 2018). Moreover, it is noteworthy that recently some mathematical efforts have been focused on studying known and novel therapies for metastasis-associated bone diseases. Such works using computational methods or optimal control theory have simulated different therapies based on: TGF-β inhibition (Cook et al. 2016; Juárez and Guise 2011), Wnt inhibition (Sousa and Clézardin 2018), chemotherapy (Lemos et al.

---

[1] The vicious cycle comprises metastasis-derived signals that stimulate bone lining osteoblasts to proliferate and/or differentiate. In response to signals derived from the metastases, the bone lining osteoblasts express osteoclastogenic factors such as RANKL, which in turn, promotes the maturation of those precursors into active osteoclasts. Since bone is rich in growth factors (TGF$-\beta$), resorption by the osteoclasts results in the increased bioavailability of TGF$-\beta$. Taken together, these osteoclast-generated factors facilitate the growth and expansion of the metastases thus completing the vicious cycle (Lynch 2011).

2016) and anti-resorptive treatment (denosumab) with radiotherapy (Camacho and Jerez 2019). Finally, some authors have used a PDE framework to study bone diseases and bone metastasis (Ryser et al. 2010; Araujo et al. 2014; Muñoz and Tello 2017). Mathematical models offer an opportunity to explore different control strategies and obtain insights about them.

It is important to remark that T cells play a major role in antitumor immunity. Following these findings, T-cell-based immunotherapeutic strategies for the treatment of tumor patients were developed (Cartellieri et al. 2010). Therefore, in recent years, genetic manipulations of T cells have been used to propose new treatments in cancer. A promising approach is the genetic modification of T cells with chimeric antigen receptors (CAR) and T-cell receptors (TCR) (June et al. 2018; Kalos et al. 2011; Zhao and Cao 2019). First, the patient's blood is extracted to obtain T cells. In the laboratory, T-cells are genetically modified to encode CAR or TC receptors that recognize cancer-specific antigens. Finally, the patient is inoculated with these new cells; afterward CAR or TCR T cells recognize and bind to tumor surface antigens. The whole process is called CAR or TCR therapy, see figure on CAR T-cell therapy of the Web page from National Cancer Institute (2021). CAR T-cell research initially focused on blood cancers such as B-cell acute lymphoblastic leukemia. In this cancer, CAR T-cell therapy slowed down or stopped the cancer proliferation in 82% of patients, and in more than half of them, the tumor disappeared completely (Jackson et al. 2016; Porter et al. 2011; Zhao and Cao 2019). On the other hand, for solid tumors, such as the case of cancers that cause metastasis, the surrounding microenvironment reduces the immune response due to immunosuppressive cells that protect the tumor tissue (Newick et al. 2016; Zhao and Cao 2019). However, clinical cancer research continues looking for the right antigen to obtain a suitable therapy for solid tumors (Rosenberg 2011). Although CAR T treatment is promising for blood cancers and solid tumors, side effects such as cytokine release syndrome (CRS) and neurological toxicities must be taken into account, an aspect that has not been studied in depth (June et al. 2018; Newick et al. 2016). It is hoped that toxicities will be anticipated and manageable, allowing for improved quality and benefit of treatment (Bonifant et al. 2016), enhanced efficacy in solid tumors (Ma et al. 2019).

It is likely that CAR T cell therapies are more cost-effective than current standard-of-care therapies for cancer. The customized manufacturing processes now used for highly personalized engineered T-cell therapies incur high costs. When the commercialization of CAR T cells is established, the costs will decrease making it a more accessible treatment. In the next years, the cost of manufacturing CAR T cells is expected to decrease (June et al. 2018; Sarkar et al. 2019). For the reasons above, it is useful to build mathematical models that incorporate the effectiveness and toxicity of CAR T cell therapy in solid tumors in order to evaluate the safety and efficacy of these complex therapies and give support to preclinical studies prior to clinical trials in humans.

In this paper, we propose a biochemical-simplified model to describe the *vicious cycle* of bone metastasis by considering power-law autocrine/paracrine growth functions of osteoclasts, osteoblasts and cancer cells. Via a bifurcation analysis we obtain parameter values for our base osteoclast-osteoblast model for three different human life stages: childhood, young adulthood, and adulthood. We investigate the link between cancer proliferation and the BMUs activation, since it is different for these three life

stages (Heaney 2001): bone remodeling period in growing children is of several weeks duration; in young adult, approximately 3 months; and in elder people, from 6 to 18 months. Bone metastases are more common in older adults, whereas bone cancer such as osteosaracoma mostly occurs in teens, though it can occur at any age. Although different cancers affect different age groups, we do not consider a specific type of cancer since our work focuses on presenting how different dynamics of the BMU affects the growth of cancer. By numerical simulations we show different behaviors of the cancer cell population in each stage. Then, we propose an optimal control problem based on our biochemical-simplified model in order to describe an antigen receptor therapy of the CAR or TCR type for bone metastasis. Numerical simulations are presented in order to illustrate different treatment efficiencies.

The paper is organized as follows: In Sect. 2 we will introduce the bone remodeling model and we will propose the parametric intervals for each human life stage based on a qualitative theoretical bifurcation analysis. In Sect. 3 we will construct a mathematical model for bone metastasis disease and an equilibrium analysis will be carried out. Numerical solutions for our bone metastasis model will be shown for the three age stages (childhood, young adulthood, and adulthood) in order to illustrate the different behaviors. In Sect. 4 from the previous model we will propose an optimal control model in order to simulate an antigen receptor treatment and the existence of optimal solutions will be proven. Solution profiles under such treatment will be also provided and a discussion of our results will be presented in Sect. 5.

2 Bone remodeling model

Here we present a basic bone remodeling (BR) model first proposed in Komarova et al. (2003), which is the basis for our bone metastasis model. Based on the kinetic interactions that exist between osteoclast and osteoblast cells, models based on power-law functions have been used to capture the relationship between those cells. These biological complex systems are comprised of numerous richly interacting components. Nevertheless, the details of the processes that govern the interactions of these components usually are not known in depth. Consequently, their description requires, as we mentioned before, a general representation to capture the core of the observed response and it should be amenable to a systematic mathematical analysis. One approach that satisfies these requirements is the power law based models (Voit 1991). Such models emerge when non-integer kinetic orders are used. Moreover, a useful property of power-law models is their ability to model the mechanism of inhibition with simplified equations, such is the case in some signals that occur in the interaction of the osteoblast and osteoclast cells; providing a general theoretical framework for addressing questions about regulation and dynamic properties of the biochemical pathways (Vera et al. 2007; Voit 1991).

Thus, based on the interactions between the osteoclast and osteoblast cell populations and their temporal changes, the BR model is written as

$$\frac{dC(t)}{dt} = \alpha_1 C^{g_{11}}(t) B^{g_{12}}(t) - \beta_1 C(t),$$

$$\frac{dB(t)}{dt} = \alpha_2 C^{g_{21}}(t) B^{g_{22}}(t) - \beta_2 B(t), \tag{1}$$

where $C(t)$ and $B(t)$ denote the number of osteoclasts cells (OC) and osteoblasts cells (OB), respectively (notice that these two variables are dimensionless); α_i is the rate of cell production for $i = 1, 2$; β_i is the rate of cell removal; the parameters g_{11} and g_{22} describe the osteoclasts and osteoblasts autocrine regulation, respectively; while g_{12} and g_{21} are parameters that describe paracrine regulation (g_{12} considers osteoblasts inhibition of osteoclasts production and g_{21} considers osteoclast regulation of osteoblasts).

System (1) has a unique equilibrium point given by

$$C^* = \left(\frac{\beta_1}{\alpha_1}\right)^{\frac{1-g_{22}}{g}} \left(\frac{\beta_2}{\alpha_2}\right)^{\frac{g_{12}}{g}}, \quad B^* = \left(\frac{\beta_1}{\alpha_1}\right)^{\frac{g_{21}}{g}} \left(\frac{\beta_2}{\alpha_2}\right)^{\frac{1-g_{11}}{g}},$$

where $g = g_{12}g_{21} - (1 - g_{11})(1 - g_{22})$. The condition for sustained oscillations (Komarova et al. 2003; Zumsande et al. 2011) is given by

$$\beta_1(g_{11} - 1) + \beta_2(g_{22} - 1) = 0. \tag{2}$$

In Jerez and Chen (2015), authors proved that the BR model with positive initial conditions and assuming $g_{12} < 0$, $g_{21} > 0$ and $g_{11} = g_{22} = 1$ has a unique positive periodic solution which oscillates around the equilibrium point. The periodicity in BMU dynamics indicates that the remodeling process occurs at a certain frequency depending on the human life stage of interest. In adults, the interval between successive remodeling events at the same location is approximately 2 years (Eriksen 2010; Manolagas 2000). Our model focuses on local bone remodeling on a spatial surface of cancellous bone on the scale of a single BMU.

The following percentage bone mass equation (Ayati et al. 2010; Jerez and Camacho 2018)

$$\frac{dz(t)}{dt} = -k_1\sqrt{\max\{C(t) - C^*, 0\}} + k_2\sqrt{\max\{B(t) - B^*, 0\}}, \tag{3}$$

is also considered with system (1) in order to calculate the bone mass percentage. Function $z(t)$ is the percentage bone mass, and parameters k_1, k_2 are the normalized activities of bone resorption and formation.

The bone remodeling process is different in each stage of human life. In children bone remodeling is a continuous process because their BMU remains more active, while in young adults and elders the remodeling process is only for skeleton maintenance, hence, the BMU remains less active (Bayliss et al. 2012; Eriksen 2010; Walsh 2015). Since our goal is to investigate the role of the frequency of OC-OB oscillations in bone metastasis disease at each stage of human life, we first carry out a bifurcation analysis ("Appendix A") to determine the parameters of system (1) in each human life cycle of interest (see Table 1). We consider three stages: childhood, young adulthood and adulthood (after 35-40 years old). Moreover, we identify that the important bifurcation parameters are g_{ij}, $i, j = 1, 2$.

Table 1 Parameter values of system (1)–(3) for childhood, young adulthood and adulthood, c=cells

Parameter	Stage			Units
	Childhood	Young adulthood	Adulthood	
α_1	0.4	0.3	0.3	day^{-1}
α_2	0.1	0.1	0.1	day^{-1}
β_1	0.2	0.2	0.2	day^{-1}
β_2	0.02	0.02	0.02	day^{-1}
g_{11}	1.08	1.0	1.0	Dimensionless
g_{12}	-1.0	-0.4	-0.3	Dimensionless
g_{21}	0.5	0.5	0.4	Dimensionless
g_{22}	0.2	1.0	1.0	Dimensionless
k_1	0.01	0.07	0.07	$\%\mu\text{m}\,\text{day}^{-1}$
k_2	0.011	0.0021	0.0019	$\%\mu\text{m}\,\text{day}^{-1}$

In Fig. 1 we show BMU dynamics for each parameter set of Table 1 for system (1)–(3). For childhood (Fig. 1a), we assume that the BMU remains periodically active with a period of four months since their bones are growing up (Bayliss et al. 2012). For young adults (Fig. 1b) the BMU is active for six months and not active for seven or eight months. Finally, for the adulthood stage (Fig. 1c) the BMU remains active for eight to ten months and inactive for the same period. This division is consistent with the existing literature on the phases of bone remodeling in the human life cycles (Heaney 2001; Eriksen 2010; Walsh 2015). Some parameter values are estimated based on existing literature. (Komarova et al. 2003) used experimental data from Parfitt (1994) to estimate the rate constants of bone cell removal, that is, they used $\beta_1 = 0.2$, and $\beta_2 = 0.02$. We adjusted the rate constants α_i of bone cell formation to obtain reasonable values for cell numbers at a single remodeling site in each human stage. Finally, we chose the constants k_i for normalized activities of bone resorption (k_1) and bone formation (k_2). The parameter values in each human life stage are different due to the amplitude and frequency of osteoclast and osteoblast oscillations, in order to obtain reasonable bone mass associated with the equilibrium state. This process is repeated in the following sections for the numerical simulations.

On the other hand, it is possible to obtain a BMU that remains active and inactive for a longer period of time.

By decreasing the effect of paracrine signaling on osteoblasts (g_{21}) and decreasing the rate of bone formation (k_2), it is possible to obtain a BMU that is active for 10 months then passive for 13 months. Notice a decrease of the bone mass in the adulthood stage, see Fig. 1, which is consistent with the literature suggesting that the fracture zone begins approximately at age 55 for women and 75 years old for men (Bayliss et al. 2012).

In the following section, we introduce a bone metastasis model in order to study the dynamics of cancer cells in each of the three-stages previously described.
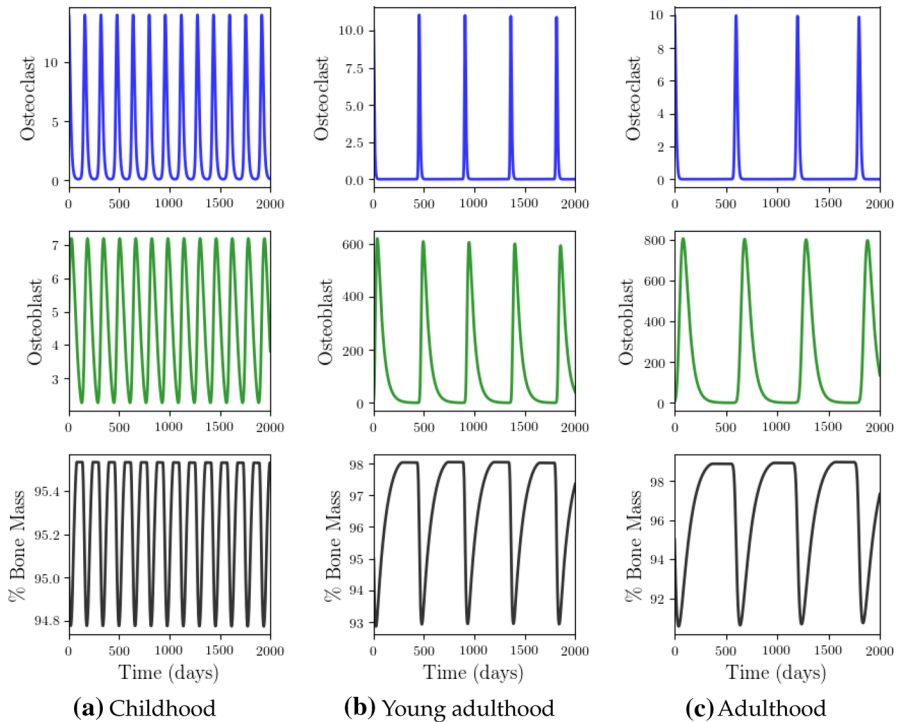
Fig. 1 Solution profiles of osteoclasts, osteoblasts and the percentage of bone mass

3 Bone metastasis model

In this section, based on the BR model (1) and considering a biochemical-simplified formulation we propose a bone metastasis (BM) model by incorporating cancer dynamics. We assume the biological assumption of the *vicious cycle* (Paget 1889; Mundy 2002) for the interplay between osteoclasts, osteoblasts and cancer cells. Summarizing, our BM model is based on the following biological considerations:

H1. The effectiveness of the paracrine/autocrine signaling between osteoclasts and osteoblasts is modeled via power-law functions as well as the paracrine signaling of cancer cells (Komarova et al. 2003; Koenders and Saso 2016; Camacho and Jerez 2019).

H2. Cancer cells have a self-limiting growth due to competition for nutrients and space. For this reason, we consider the logistic growth function to model cancer dynamics (Eladdadi et al. 2014).

H3. Sustained apoptosis of a minor component of tumor cells promotes tumor growth and progression (Wang et al. 2013). Thus a cancer apoptosis term is included and is considered proportional to the cancer cells population (Koenders and Saso 2016; Camacho and Jerez 2019).

H4. Cancer and osteoclasts have a mutualistic relationship (Mundy 2002; Ottewell 2016).

H5. Cancer and osteoblasts have a mutualistic or competitive relationship depending on growth factors (TGF-β and TNF-α) (Mundy 2002; Camacho and Pienta 2014).

Thus, based on those previous assumptions we propose the following model

$$
\begin{aligned}
\frac{dC(t)}{dt} &= \alpha_1 C(t)^{g_{11}} B(t)^{g_{12}} - \beta_1 C(t) + \sigma_1 C(t) T(t), \\
\frac{dB(t)}{dt} &= \alpha_2 C(t)^{g_{21}} B(t)^{g_{22}} - \beta_2 B(t) + \sigma_2 B(t) T(t), \\
\frac{dT(t)}{dt} &= \alpha_3 C(t)^{g_{31}} T(t) \left(1 - \frac{T(t)}{K} \right) - \beta_3 T(t),
\end{aligned}
\tag{4}
$$

where $C(t)$, $B(t)$ and $T(t)$ denote biomass of osteoclasts, osteoblasts and cancer cells at time t, respectively. α_3 is the rate of cancer cell production; β_3 is the rate of cancer cell removal; σ_1 and σ_2 are the proportional rates of the osteoclasts-cancer and osteoblasts-cancer interaction where we incorporate the vicious cycle; the coefficient K is the carrying capacity of the logistic growth rate of cancer cells within the BMU location; g_{31} describes the effects of the complex biochemical reactions between osteoclasts and cancer cells. We assume that osteoclast cells promote cancer cells growth, which implies that $g_{31} > 0$.

Let Ω be the set $\{(C, B, T) : C, B > 0, \ T \geq 0\} \subset \mathbb{R}_+^3$. For system (4), we only consider parameter values where the functions on the right side are locally Lipschitz continuous with respect to $(C(t), B(t), T(t))$ in Ω, so that for any initial condition $(C_0, B_0, T_0) \in \Omega$ there exists a unique solution which belongs to the positively invariant set Ω.

3.1 Equilibrium and stability analysis

In this section, we give the stationary solutions of the BM model (4) along with their stability conditions when $g_{11} = g_{22} = 1$. The equilibria of this system consist of two steady-states points: the cancer-free equilibrium and the cancer-invasion equilibrium. The cancer-free equilibrium is given by

$$
(C_F^*, B_F^*, T_F^*) = \left(\left(\frac{\beta_2}{\alpha_2} \right)^{\frac{1}{g_{21}}}, \left(\frac{\beta_1}{\alpha_1} \right)^{\frac{1}{g_{12}}}, 0 \right).
\tag{5}
$$

The cancer-invasion equilibrium is given by (C_I^*, B_I^*, T_I^*) where

$$
C_I^* = \left(\frac{\beta_2 - \sigma_2 T_I^*}{\alpha_2} \right)^{\frac{1}{g_{21}}}, \quad B_I^* = \left(\frac{\beta_1 - \sigma_1 T_I^*}{\alpha_1} \right)^{\frac{1}{g_{12}}} \ \text{and}
$$

$$
T_I^* = K \left(1 - \frac{\beta_3}{\alpha_3} \left(\frac{\beta_2 - \sigma_2 T_I^*}{\alpha_2} \right)^{\frac{-g_{31}}{g_{21}}} \right).
\tag{6}
$$

If also $g_{21} = g_{31}$, then the cancer-invasion equilibrium can be expressed as:

$$C_I^* = \left(\frac{\beta_2 - \sigma_2 T_I^*}{\alpha_2}\right)^{\frac{1}{g_{21}}}, \quad B_I^* = \left(\frac{\beta_1 - \sigma_1 T_I^*}{\alpha_1}\right)^{\frac{1}{g_{12}}} \text{ and}$$

$$T_I^* = \frac{(\beta_2 + \sigma_2 K) \pm \sqrt{(\beta_2 + \sigma_2 K)^2 - 4\sigma_2 K \left(\beta_2 - \frac{\alpha_2 \beta_3}{\alpha_3}\right)}}{2\sigma_2}. \tag{7}$$

In the following we analyze the stability of equilibrium states (5) and (7).

3.1.1 Cancer-free equilibrium

The roots of the characteristic polynomial associated with the cancer-free equilibrium (5) are

$$\lambda_1 = \alpha_3 \left(\frac{\beta_2}{\alpha_2}\right)^{\frac{g_{31}}{g_{21}}} - \beta_3; \quad \lambda_2 = i\sqrt{g_{12}g_{21}\beta_1\beta_2}; \quad \lambda_3 = -i\sqrt{g_{12}g_{21}\beta_1\beta_2}. \tag{8}$$

Since λ_2 and λ_3 have real part zero, the stability of the equilibrium point depends only on λ_1. For $\lambda_1 > 0$, the steady state is unstable but if $\lambda_1 < 0$ then linear analysis is not conclusive. However, when the cancer-free equilibrium is reached system (4) becomes a particular case of BR model 1 where a periodic solution is obtained, see (Jerez and Chen 2015).

Theorem 1 *System* (4) *with any initial condition* $(C_0, B_0, T_0) \in \Omega$ *and verifying* $g_{12} < 0$ *and* $g_{21} > 0$ *has a locally stable cancer-free equilibrium solution if* $\left(\frac{\beta_2}{\alpha_2}\right)^{\frac{g_{31}}{g_{21}}} < \frac{\beta_3}{\alpha_3}$.

Moreover, system (4) *has a unique periodic solution. If* $\left(\frac{\beta_2}{\alpha_2}\right)^{\frac{g_{31}}{g_{21}}} < \frac{\beta_3}{\alpha_3}$ *is not satisfied then the cancer-free equilibrium is unstable.*

Proof Inequality $\left(\frac{\beta_2}{\alpha_2}\right)^{\frac{g_{31}}{g_{21}}} < \frac{\beta_3}{\alpha_3}$ is obtained forcing to satisfy $\lambda_1 < 0$ and the periodicity of the solution is guaranteed by Theorem 3.1 in (Jerez and Chen 2015). □

3.1.2 Cancer-invasion equilibrium

To analyze the stability of this equilibrium point we use Routh-Hurwitz criterion (Wiggers and Pedersen 2018).

Theorem 2 *Let system* (4) *with any initial condition* $(C_0, B_0, T_0) \in \Omega$ *and verifying* $g_{12} < 0$, $g_{21} > 0$ *and* $g_{21} = g_{31}$. *Then, the cancer-invasion equilibrium* (7) *is locally asymptotically stable if* $\sigma_2 > 0$, $\frac{\beta_3}{\alpha_3} < \frac{\beta_2}{\alpha_2}$ *and* $\frac{|g_{12}\sigma_2|\beta_1}{\sigma_1\alpha_3} + \frac{\beta_3}{\alpha_3} < \frac{\beta_2}{\alpha_2}$. *Moreover,* (7) *is unstable if* $\sigma_2 < 0$.

Proof To get all the roots of the characteristic polynomial with negative real part, we impose the Routh-Hurwitz criterion, then $\sigma_2 > 0$, $\frac{\beta_3\alpha_2}{\alpha_3} - \beta_2 < 0$, $\sigma_1\beta_2 - \frac{|g_{12}\sigma_2|\alpha_2}{\alpha_3} -$

Table 2 Parameter values for cancer-free dynamics in bone metastasis model (3)–(4) for the three stages

Parameter	Cancer-free	Units
α_3	0.053	day^{-1}
β_3	0.05	day^{-1}
σ_1	0.001	day^{-1}
σ_2	0.00005	day^{-1}
g_{31}	0.01	Dimensionless
k_1	0.07	%µm day^{-1}
k_2	0.0023	%µm day^{-1}

Table 3 Parameter values for cancer-invasion dynamics in bone metastasis model (3)–(4)

Parameter	Cancer-invasion Scenario A1	Scenario A2	Units
α_3	0.052	0.065	day^{-1}
β_3	0.05	0.05	day^{-1}
σ_1	0.001	0.002	day^{-1}
σ_2	-0.005	0.00005	day^{-1}
g_{31}	0.01	0.02	Dimensionless
k_1	0.02	0.05	%µmday^{-1}
k_2	0.005|0.023	0.0025	%µm day^{-1}

$\frac{\beta_3 \sigma_1 \alpha_2}{\alpha_3} > 0$ and we get $T_I^* > 0$. Otherwise, if $\sigma_2 < 0$ the second condition in such criterion is never satisfied and the cancer-invasion equilibrium is unstable.   □

Notice that when the condition $\frac{\beta_3}{\alpha_3} < \frac{\beta_2}{\alpha_2}$ is satisfied, we have from Theorem 1 that the cancer-free equilibrium is unstable.

3.2 Numerical results

In this section, we show numerical simulations of the bone metastasis model (4) along with the bone mass equation (3). In order to illustrate the solution's behavior of OCs, OBs and cancer cells in childhood, young adult, and adulthood, we reuse the parameter values given in Table 1. In particular, we show cancer-free dynamics and cancer-invasion dynamics for the bone metastasis disease for the three human life stages of interest. In Tables 2 and 3, we give the growth and death rates of cancer cells and the values of BMU-cancer interaction parameters, σ_1 and σ_2, for different scenarios of the cancer-free and cancer-invasion dynamics, respectively. The rate of cancer cell production, α_3, and the rate of cancer cell removal, β_3, have been chosen according to the values proposed in the literature (Ayati et al. 2010; Koenders and Saso 2016; Farhat et al. 2017). Parameters σ_1 and σ_2 have been estimated by considering stability conditions of Theorems 1 and 2. For g_{31}, we explored the high/low paracrine activity taking into consideration data given in Koenders and Saso (2016). Finally, we
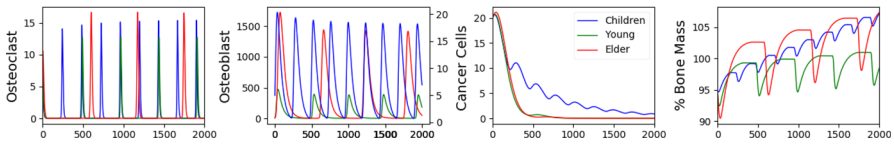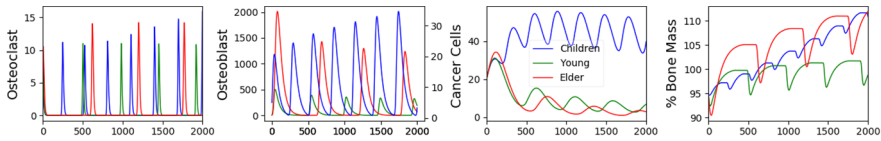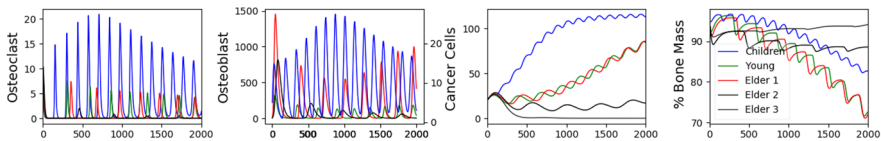
Fig. 2 Cancer-free behavior of bone metastasis model (3)–(4) for childhood, young adult, and adulthood stages with initial condition $(C, B, T, z) = (10, 5, 20, 95)$ representing an ending/beginning of the active obsteoclast/osteoblast stage in presence of few tumor cells

(a) $\alpha_3 = 0.06$ and the rest of parameters in Table 2.

(b) $\alpha_3 \in [0.055 - 0.057]$, $\beta_3 = 0.05$, $\sigma_1 = 0.001$, $\sigma_2 = -0.0005$, $g_{31} = 0.01$, $k_1 = 0.07$ and $k_2 = 0.0013$ (children: $k_1 = 0.02$ and $k_2 = 0.01$).

Fig. 3 Cancer-invasion behavior of bone metastasis model (3)–(4) for childhood, young adult, and adulthood stages with initial conditions $(C, B, T, z) = (10, 5, 20, 95)$. However, if the BMU remains less active, non-invasive cancer is possible (see Elder-2-3 black lines)

estimated the value of the carrying capacity of the cancer cells as $K = 1000$ according to Farhat et al. (2017).

Figure 2 shows the behavior of osteoclasts, osteoblasts, cancer cells, and the bone mass percentage for childhood, young adult, and adulthood stages. In the three stages, a cancer-free dynamic is presented and cancer cells display unstable oscillations that converge to the trivial steady-state. In spite of a null cancer invasion, there is a little bone damage owing to overstimulation of osteoblast cells in childhood and adulthood stages which is noticed by the bone mass increasing. Observe that an osteoblastic lesion in the three-stages is presented. Moreover, if we slightly increase the cancer growth rate, α_3, given in Table 2, we have cancer invasion in the childhood population while in the young adults and adulthood cancer invasion does not occur (Fig. 3a). Thus, we could consider that in childhood a cancer invasion is more feasible under the same environmental conditions.

On the other hand, in Fig. 3 we show cancer-invasion dynamics in the three human life stages. We can observe that the dynamics of cancer in childhood is faster than in the young adult or adulthood stages, which is consistent with the literature (Ghaderi et al. 2012). Nevertheless, it would be interesting to explore what happens when the BMU becomes gradually less active. For this we consider two different study cases *Elder-2* and *Elder-3*, both of which are special study cases since in them the BMU remains inactive for more than 10 months. In our simulations, we obtain that if the BMU
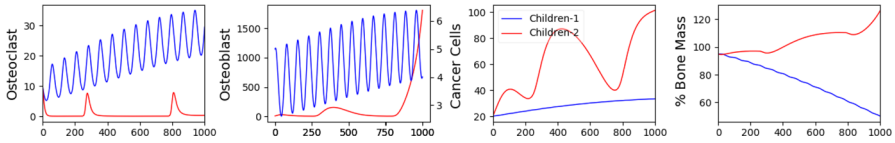
Fig. 4 Cancer-invasion solution behaviors of bone metastasis model (3)–(4) for childhood with initial conditions $(C, B, T, z) = (10, 5, 20, 95)$. Scenario 1: Blue line, Scenario 2: Green line and Scenario 3: Red line (colour figure online)
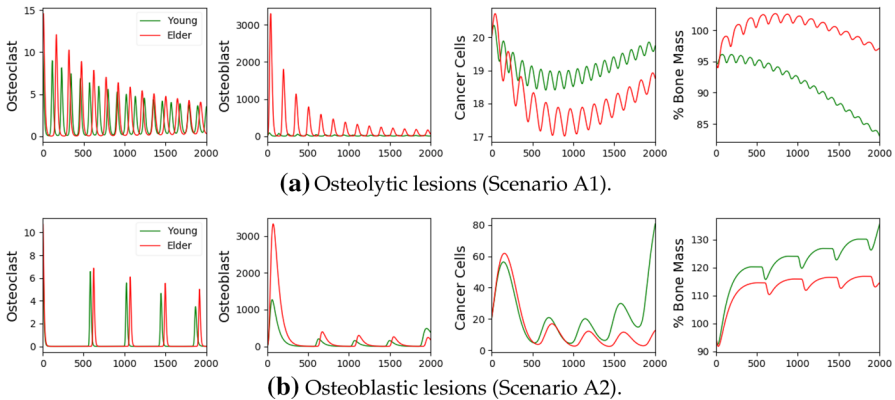

(a) Osteolytic lesions (Scenario A1).

(b) Osteoblastic lesions (Scenario A2).

Fig. 5 Cancer-invasion solution behaviors of bone metastasis model (3)–(4) for young adult and elder with initial conditions $(C, B, T, z) = (10, 5, 20, 95)$ and under the parameter values of Table 3

remains active and inactive for a long period, the cancer invasion is slow or it does not even occur. That is, when considering "adulthood" values in Table 1 cancer invasion and osteolytic lesions are present (Elder-1), however, when we modified the values g_{12} and g_{21} cancer invasion and osteolysis does not occur, see Fig. 3b ($g_{12} = -0.4$, $g_{21} = 0.2$ and $g_{21} = 0.1$ for Elder-2 and Elder-3, respectively.) Therefore, in elders, increasing the inhibitory effect of OB on OC (g_{12}) and decreasing the stimulating effect of OC on OB (g_{21}) prevented cancer invasion and osteolytic lesions.

We present now osteoblastic and osteolytic lesions associated with bone metastasis, which result in bone diseases like osteoporosis and osteopetrosis (Mundy 2002). In order to obtain both lesions, we take the parameter values of Table 3. The choice of the parameters is within the ranges presented in the literature (Ayati et al. 2010; Farhat et al. 2017; Koenders and Saso 2016). Under cancer-invasion conditions, we consider two scenarios: an osteolytic lesion (*Scenario A1*) and osteoblastic lesions (*Scenarios A2*), see Table 3. Despite having two different bone lesions in *Scenarios* A1 and A2, there is evidence of the adaptation period that cancer needs before it shows a more accelerated spread, see plot of cancer cells in Fig. 5a, b . Taking into account that the invasion time of cancer is different for children than for adults, we show BMU-cancer dynamics in different figures. In Fig. 4 we show the two scenarios for childhood stage, considering 1000 days since the BMU is destroyed after that time. Notice that cancer-invasion strongly affects osteoclast cells in *Scenario A1* and osteoblast cells in *Scenario A2* causing severe damage to the bone mass. According to the literature on

malignant bone tumors in childhood, the peak incidence is at age 15, which coincides with adolescent growth spurts. This fact supports our model since all simulations have shown that the accelerated growth and invasion of the metastasis is obtained when the BMU remains more active, which occurs in the growth stage, i.e. in the childhood stage (Weiner et al. 2003). On the other hand, in Fig. 5 we present cancer-invasion dynamics for young adults and adults by considering values of Table 3. We can observe that BMU cells and cancer cells have very similar solution behaviors at both stages. Nevertheless, the changes in the wave amplitudes are more drastic in young adults than adults. Moreover, it is interesting the behavior of cancer which presents fluctuations in their solution curves. This can be explained by the unstable tumor growth associated with early metastatic tumor stages. Metastatic tumors are complex biosystems; cancer cells undergo a period of adaptation before metastasizing the bone to avoid destruction by the immune cells (Gonzalez et al. 2018; Randall et al. 2016; Rhodes and Hillen 2019, 2020).

In order to propose a novel treatment for bone metastasis, in the next section we will construct a mathematical model based on an antigen receptor therapy of the CAR or TCR type using optimal control theory.

4 Optimal control model: antigen receptor therapy

Infusion of T cells directed against specific antigens holds great promise in cancer therapy, and this approach is triggering a paradigm shift in cancer immunotherapy. One of the most exciting of these approaches has been the use of T cells that have been genetically engineered to express chimeric antigen receptors (CAR) that target an antigen on the surface of a tumor (Newick et al. 2016), and they are the first form of gene transfer therapy to gain commercial approval (June et al. 2018). The transfer of CAR T cells has demonstrated remarkable success in treating blood-borne tumors, and as a consequence a growing number of clinical trials have focused on solid tumors, targeting surface proteins (Gilham et al. 2012). However, CAR T therapy has not been as successful in solid tumors due to the limited ability of CAR T cells to infiltrate the tumor and the immunosuppressive microenvironment (Hillerdal and Essand 2015). Furthermore, CAR T cell therapy must be used carefully due to the risk of cytokine release syndrome (CRS) (which is correlated with tumor burden) and neurologic toxicities. Despite these limitations, CAR T cell therapy has the potential to be used to treat solid tumors, and there have been a few positive results in clinical trials for solid tumors including neuroblastoma and sarcoma (Newick et al. 2016).

The main essence of this treatment is that CAR T cells cause apoptosis of cancer cells by binding to receptors on the surface of cancer cells. Below, we incorporate this effect into our mathematical model, which subsequently breaks the *vicious cycle* of bone metastasis. Thus, in order to eliminate cancer cells and try to break the *vicious cycle* of bone metastasis, we propose an optimal control problem based on the bone metastasis model (4). Our model is consistent with a therapy of the CAR or TCR type and assumes the following:

H6. The main effect of an antigen receptor therapy is that apoptosis is trigged when the modified cells (CAR T cells) interact with cancer cells (Zhao and Cao 2019).

H7. In solid tumors this therapy is less effective than in blood cancer since the components of the surrounding microenvironment conspire to mitigate the immune response(Newick et al. 2016; Zhao and Cao 2019).

H8. Antigen receptor cells have an important limitation that there are very few antigens on the tumor cells surface for which a binding affinity can be reached, but once they tethered to a cancer cell they can eliminate it (He et al. 2019).

H9. The CAR T cells have been modified to improve trafficking to the tumor, which also has a direct effect on osteoclasts (Hillerdal and Essand 2015) and osteoblasts.

The effect function of an antigen receptor therapy, denoted by $u(t)$, is included into the bone metastasis model (4) in order to minimize the cancer cells population as well as the cost of control effort. Given the previous assumptions, we propose the following antigen receptor model:

$$\min_{u} J(T, u) = \int_{0}^{t_f} \left(T(t) + \frac{A}{2} u^2(t) \right) dt, \tag{9}$$

subject to the controlled dynamical system

$$\frac{dC(t)}{dt} = \alpha_1 C(t)^{g_{11}} B(t)^{g_{12}} - \beta_1 C(t) + (\sigma_1 - a_1 u(t)) C(t) T(t), \tag{10a}$$

$$\frac{dB(t)}{dt} = \alpha_2 C(t)^{g_{21}} B(t)^{g_{22}} - \beta_2 B(t) + (\sigma_2 - a_2 u(t)) B(t) T(t), \tag{10b}$$

$$\frac{dT(t)}{dt} = \alpha_3 C(t)^{g_{31}} T(t) \left(1 - \frac{T(t)}{K} \right) - (\beta_3 + u(t)) T(t), \tag{10c}$$

where

$$u(t) : [0, \ t_f] \mapsto [0, \ u_c], \tag{11}$$

with t_f the final time of the treatment and $u_c \in (0, 1)$ the efficiency of the antigen receptor therapy, taking into consideration that the effectiveness of the treatment in solid tumors is less than in blood cancer (see H7). Parameters a_1 and a_2 describe how the therapy could affect the surrounding microenvironment in "vicious cycle" dynamics (see H9). For example, the CAR T cells could be engineered to counteract the immunosuppressive microenvironment created by osteoclast activity (Hillerdal and Essand 2015). The weight coefficient $A > 0$ is assumed constant and it controls the effect of $u(t)$. The value of A is chosen to balance the magnitudes of the cancer cells biomass and the control function since both are in different magnitude scales. The cost functional $J(T, u)$ measures the cost per unit of time of the presence of cancer cells with the term $T(t)$ and the economical cost of using the proposed therapy with the term $u(t)^2$. It is worth pointing out that in the formulation of the optimal control

problem we have assumed a non linear relationship between the coverage of control actions and their underlying costs. Under this assumption, the integrated function in (9) is quadratic with respect to $u(t)$. The quadratic form of the objective functional $J(T, u)$ with respect to the control variable $u(t)$ clearly states that the total marginal cost of the control (that is, $Au(t)$) effectively depends on the amount of treatment. As marginal cost is the change in total cost, the integral $J(T, u)$ is quadratic with respect to the control variable. This approach is rather conventional in biological modelling where optimal control methods are applied. It has been justified for models where control functions expressed optimal treatment and/or vaccination policies (Neilan and Lenhart 2010). Additionally, the quadratic form of control in (9) helps to justify the existence of solution of the optimal control problem (9)–(10) and it allows for a rather logical and simple interpretation of the maximum principle.

It is worth noting that the optimal control problem (9)–(11) makes sense only under the conditions of Theorem 2. Nevertheless, if any condition is not satisfied we could consider a compact subset containing the cancer-invasion equilibrium from which the solution of system (4) remains in that subset for every positive time $t > 0$. Thus, let Ω be a compact subset of the domain of system (4), such that $(C(t), B(t), T(t))$ are uniformly bounded, that is, $C(t) \leq C_{max}$ and $B(t) \geq B_{min}$ for all $t \in [0, t_f]$.

4.1 Existence of an optimal solution

Let Γ be the set of admissible control functions, where

$$\Gamma = \big\{ u \mid u \text{ is piecewise continuous function on } [0, t_f] \big\}. \tag{12}$$

Here we seek for an optimal control function $u^* \in \Gamma$, such that $J(T^*, u^*) = \min\{J(T, u) \mid u \in \Gamma\}$ almost for all $t \in [0, t_f]$. In the following results, we state the existence result of optimal solutions and give its characterization.

Theorem 3 *The optimal control problem* (9)–(12) *has non-trivial solution* $u^* \in \Gamma$ *such that* $\min\limits_{u \in \Gamma} J(T, u) = J(T^*, u^*)$.

The proof of this theorem can be found in "Appendix B".

Let us now introduce the Hamiltonian function related to the optimal control problem (9)–(12). The Hamiltonian function $\mathcal{H}(C, B, T, u, \lambda_1, \lambda_2, \lambda_3) : \Omega \times \Gamma \times \mathbb{R}^3 \mapsto \mathbb{R}$ associated with the previous optimal control problem is defined as

$$
\begin{aligned}
\mathcal{H} = {} & T(t) + \frac{A}{2}u^2(t) \\
& + \lambda_1 \big[\alpha_1 C(t)^{g_{11}} B(t)^{g_{12}} - \beta_1 C(t) + (\sigma_1 - a_1 u(t))C(t)T(t) \big] \\
& + \lambda_2 [\alpha_2 C(t)^{g_{21}} B(t)^{g_{22}} - \beta_2 B(t) + (\sigma_2 - a_2 u(t))B(t)T(t)] \\
& + \lambda_3 \left[\alpha_3 C(t)^{g_{31}} T(t) \left(1 - \frac{T(t)}{K} \right) - (\beta_3 + u(t))T(t) \right],
\end{aligned}
\tag{13}
$$

where $\boldsymbol{\lambda}(t) = (\lambda_1(t), \lambda_2(t), \lambda_3(t))'$ denotes the adjoint vector-function that satisfies the adjoint dynamical system with corresponding transversality condition specified in

the endpoint of the interval $[0, \ t_f]$, that is,

$$\frac{d\boldsymbol{\lambda}}{dt} = \begin{pmatrix} -\mathcal{H}_C \\ -\mathcal{H}_B \\ -\mathcal{H}_T \end{pmatrix}, \qquad \boldsymbol{\lambda}(t_f) = \begin{pmatrix} 0 \\ 0 \\ 0 \end{pmatrix}. \tag{14}$$

Here $\mathcal{H}_C$, $\mathcal{H}_B$ and $\mathcal{H}_T$ denote the partial derivatives of function (13) with respect to C, B and T. Function $\boldsymbol{\lambda}(t)$ can be viewed as an additional benefit or cost associated with changes in the state variables. By Pontryagin maximum principle (Lenhart and Workman 2007), if u^* and the corresponding (C^*, B^*, T^*) is optimal solution to the problem (9)–(12), then there exists a piecewise differentiable adjoint function $\boldsymbol{\lambda}(t)$ satisfying (14) such that

$$\mathcal{H}(C^*, B^*, T^*, u^*, \lambda_1(t), \lambda_2(t), \lambda_3(t)) \leq \mathcal{H}(C^*, B^*, T^*, u, \lambda_1(t), \lambda_2(t), \lambda_3(t)),$$

for all $u \in \Gamma$ and almost for all $t \in [0, \ t_f]$. Thus, the following result can be formulated.

Proposition 1 *Given an optimal control $u^*(t)$, as well as the optimal states C^*, B^*, and T^* defined as solutions of corresponding dynamical system (10), then there exists an absolutely continuous adjoint vector-function $\boldsymbol{\lambda}(t) : [0, \ t_f] \mapsto \mathbb{R}^3$ such that*

$$\begin{aligned}
\frac{d\lambda_1}{dt} =\ & -\lambda_1(\alpha_1 g_{11} C^{*g_{11}-1} B^{*g_{12}}(t) - \beta_1 + (\sigma_1 - a_1 u^*(t))T^*(t)) \\
& -\lambda_2(g_{21}\alpha_2 C^{*g_{21}-1}(t) B^{*g_{22}}(t)) \\
& -\lambda_3\left(g_{31}\alpha_3 C^{*g_{31}-1}(t)T^*(t)\left(1 - \frac{T^*(t)}{K}\right)\right),
\end{aligned} \tag{15a}$$

$$\begin{aligned}
\frac{d\lambda_2}{dt} =\ & -\lambda_1(g_{12}\alpha_1 C^{*g_{11}} B^{*g_{12}-1}(t)) - \lambda_2(g_{22}\alpha_2 C^{*g_{21}}(t) B^{*g_{22}-1}(t) \\
& -\beta_2 + (\sigma_2 - a_2 u^*(t))T^*(t)),
\end{aligned} \tag{15b}$$

$$\begin{aligned}
\frac{d\lambda_3}{dt} =\ & -1 - \lambda_1(\sigma_1 - a_1 u^*(t))C^*(t) - \lambda_2(\sigma_2 - a_2 u^*(t))B^*(t), \\
& -\lambda_3\left(\alpha_3 C^{*g_{31}}(t)\left(1 - \frac{2T^*(t)}{K}\right) - (\beta_3 + u^*)\right),
\end{aligned} \tag{15c}$$

$$\lambda_1(t_f) = \lambda_2(t_f) = \lambda_3(t_f) = 0. \tag{15d}$$

Furthermore, the characterization of an optimal control function u^* can be written as

$$u^*(t) = \min\left\{\max\left\{\frac{1}{A}(a_1 C^* T^* \lambda_1 + a_2 B^* T^* \lambda_2 + T^* \lambda_3), 0\right\}, u_c\right\}. \tag{16}$$

Proof Notice that the adjoint system (15) can be directly obtained from (14). Optimal control functions $u^*(t)$ minimize the Hamiltonian function $\mathcal{H}$ over $u \in \Gamma$. Therefore, it must comply with the necessary optimality condition, that is, $\mathcal{H}_u = 0$ whenever $u^* \in \Gamma$ or takes values on the boundary of the admissible control set Γ. Finally, given

Table 4 Parameter values of bone metastasis model (4) for aggressive bone metastasis

Parameters	g_{31}	α_3	β_3	σ_1	σ_2	K
Scenario B1	0.1	0.0017	0.001	0.00001	−0.001	5000
Scenario B2	0.1	0.005	0.0001	0.00005	0.000001	5000

that $u(t)$ is a bounded function, the necessary optimality condition can be expressed in the following form (Lenhart and Workman 2007):

$$\begin{cases} Case\ 1: If\ \mathcal{H}_u > 0\ for\ all\ u \in [0, u_c],\ then\ u^* = 0, \\ Case\ 2: If\ there\ exists\ a\ u \in [0, u_c]\ such\ that\ \mathcal{H}_u = 0,\ then\ u^* = u, \quad (17) \\ Case\ 3: \mathcal{H}_u < 0\ for\ all\ u \in [0, u_c],\ then\ u^* = u_c \end{cases}$$

Taking into account that $\mathcal{H}_u = Au - \lambda_1 a_1 CT - \lambda_2 a_2 BT - \lambda_3 T$, we can rewrite (17) in the compact form (16) and obtain the optimal control characterization. □

The forthcoming section is devoted to evaluate the effectiveness of the antigen receptor therapy for the bone metastasis disease modeled by system (9)–(10).

4.2 Numerical results

In the following, we show numerical solutions of the optimal control problem (9)–(11) in order to analyze a possible antigen receptor therapy for bone metastasis. Due to the non-linearity of the optimal-adjoint systems (10)–(15), they can only be approximated numerically. The theoretical results of the above section ensure that if the numerical method is convergent, the numerical solution is an optimal solution of the problem (9)–(11). Here we use a standard numerical method, the forward-backward sweep method, for more details see (Lenhart and Workman 2007).

In particular, we analyze the proposed therapy in late stages of cancer since the CAR T-cell therapy is given in these stages when patients are not responding to common cancer treatments (chemotherapy, radiotherapy, etc.) or it is not possible to apply them (Klebanoff et al. 2014; Zhao and Cao 2019). Table 4 presents parameter values of system (4) for aggressive bone metastasis, where the *Scenario B1* set is linked with unstable osteoclast-osteoblast oscillations and the *Scenario B2* set is linked with one or two stable osteoblast waves. These values have been chosen in such a way that they satisfy the conditions of Theorem 2 for the unstable and stable cancer-invasion equilibrium. Furthermore, in the stable *Scenario B2* it is possible to recover the dynamics of a healthy BMU with the appropriate optimal control. We consider $a_1 = a_2 = 0.00001$, which relates to the efficacy of the *vicious cycle* breaking between the BMU cells and cancer cells. The weight coefficients in the objective functional (9) is proposed as $A = 1000$. We will show numerical simulations considering different efficiencies of the therapy (that is, different values of u_c) for the three human life stages: childhood, young adult and adulthood stages.

Figures 6, 7 and 8 show the solution profiles of BMU cells and cancer cells with and without treatment in children, young adults, and adults respectively for a period of
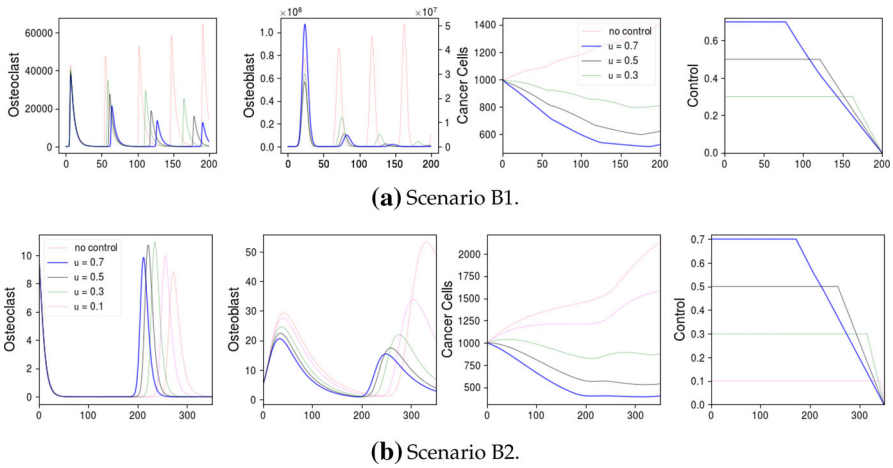
(a) Scenario B1.

(b) Scenario B2.

Fig. 6 Optimal trajectories of osteoclasts, osteoblasts, cancer cells and antigen receptor control function of therapy model (9)–(10) for the childhood stage. On top OB graph the right scale is only for the blue curve (colour figure online)
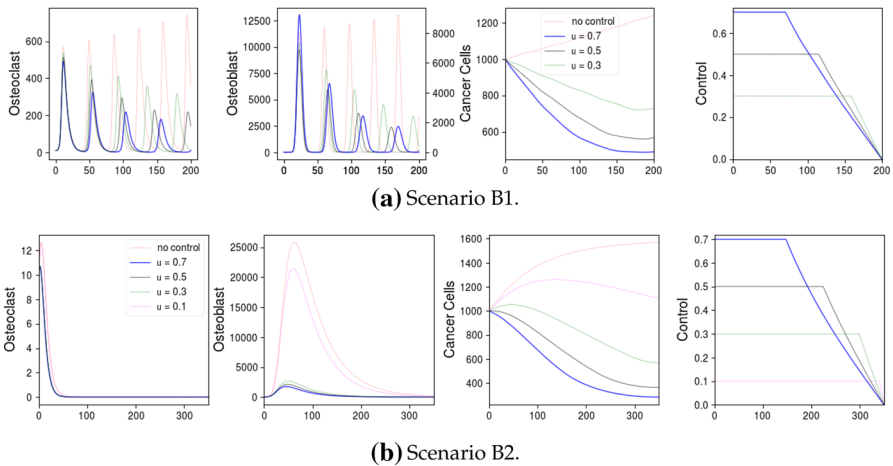

(a) Scenario B1.

(b) Scenario B2.

Fig. 7 Optimal trajectories of osteoclasts, osteoblasts, cancer cells and antigen receptor control function of therapy model (9)–(10) for the young adult stage. On top OBs graph the right scale is only for the blue curve (colour figure online)

350 days. In *Scenario B1* the behavior of osteoclasts and osteoblasts without control shows unstable oscillations (see red lines). Notice that for this scenario if we consider an effectivity of 10% ($u_c = 0.1$) of the antigen receptor therapy in the three human life stages it stays active most of the time and at the end it is suspended abruptly (see magenta lines). On the other hand, when a therapy effectivity of 70% ($u_c = 0.7$) is considered then the antigen receptor treatment lasts 150 days, after that, it gradually decreases (see blue lines). The qualitative behavior of the state variables and the control function is similar in the three stages. However, it is important to point out that cancer-
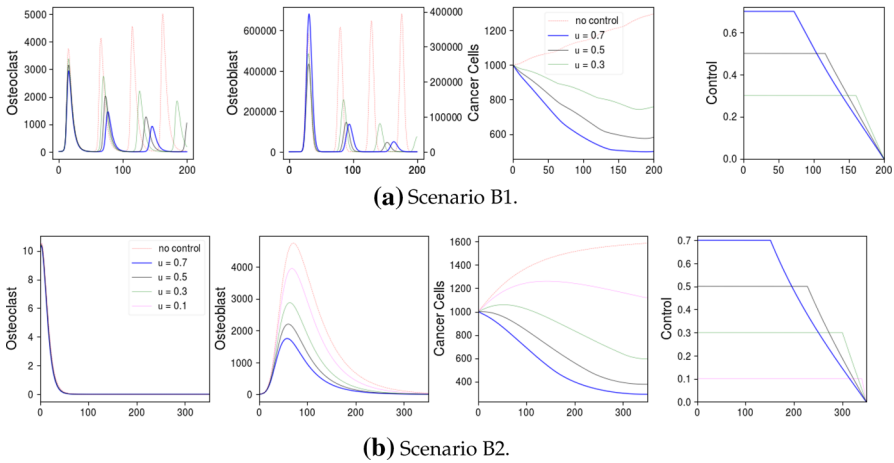
(a) Scenario B1.

(b) Scenario B2.

Fig. 8 Optimal trajectories of osteoclasts, osteoblasts, cancer cells and antigen receptor control function of therapy model (9)–(10) for the elder stage. On top OBs graph the right scale is only for the blue curve (colour figure online)

invasion is more aggressive in the childhood stage than in the others. It is interesting that in cases where the effectiveness is higher (70%), the response to the treatment is slightly better in the childhood stage than in the adulthood stages. In *Scenario B2*, there is an osteoblastic lesion in the case of adult patients with an intermediate effectivity of the treatment, normal values of osteoclasts and osteoblasts are recovered with a significant reduction in cancer cells (Fig. 8b). On the other hand, for children an osteolytic lesion is observed and normal values for the osteoclast and osteoblast cells are not recovered (Fig. 8b). We could conjecture that tumor related with osteolytic lesions may be more difficult to control with an antigen receptor treatment. Moreover, in both *Scenarios* the optimal solution remains constant for a certain period and then gradually decreases. This result makes biological sense according to what is observed in the treatments with CAR T cells. Treatment is typically given as a one-time infusion, after which the engineered cells expand within the patient's body to kill the tumor. The cellular kinetics of CAR-T therapy varies but generally peaks early and declines over time (US Food and Drug Administration 2021).

For both scenarios, the number of cancer cells is drastically reduced if we consider an efficiency greater than 30%. In comparison, clinical trials have shown an efficacy of 28% in neuroblastoma and sarcoma treatment (Ahmed et al. 2015; Louis et al. 2011). However, in the numerical simulations cancer is still present during the treatment over a period of approximately 350 days. Nevertheless, if the effectiveness is greater than 50%, the decrease in the number of cancer cells occurs between 50-100 days of treatment in both scenarios. In comparison, in clinical trials for multiple myeloma the median tumor response time was 30 days (Business Wire 2021).

It is important to point out that in the case of *Scenario B1*, the oscillations of osteoclasts and osteoblasts are unstable which makes difficult to recover normal BMU dynamics, see Fig. 9. In this case, we may consider that an additional RANKL/OPG inhibition or reactivation treatment would be required. Interestingly, in simulations
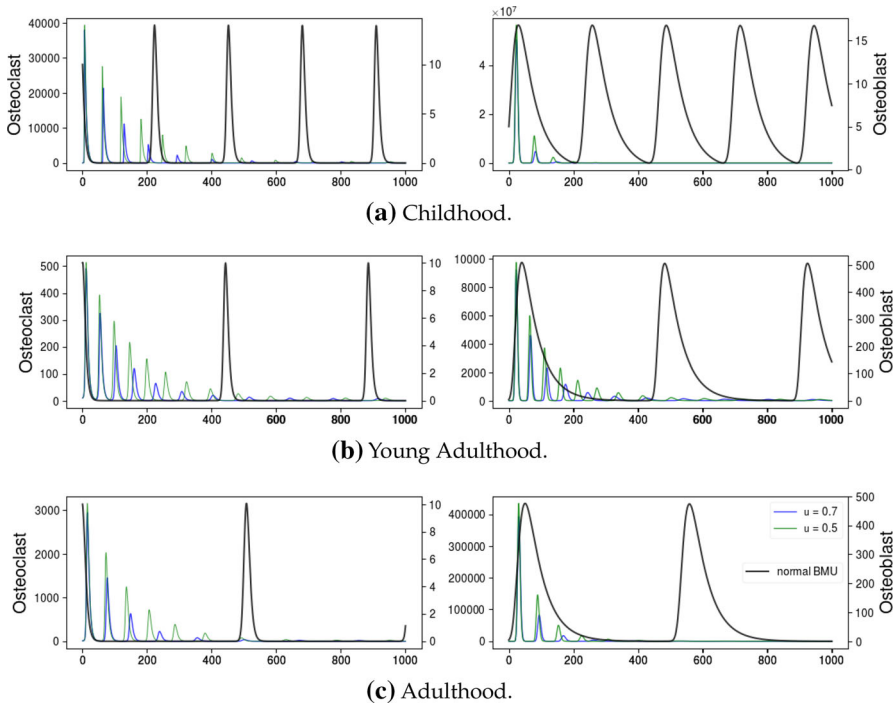
(a) Childhood.

(b) Young Adulthood.

(c) Adulthood.

Fig. 9 Comparison of a normal BMU with the osteoclasts and osteoblasts solution profiles given by the CAR-T cell therapy model under the *Scenario B1* considering effectivities of 50% and 70%. The right scale is only for a BMU normal

of *Scenario B2* considering an effectiveness greater than 30%, the use of an antigen receptor therapy allows the gradual recovery of normal BMU dynamics associated with a significant reduction of cancer in all three stages, see Fig. 10.

In summary, this type of treatment would break the *vicious cycle* of bone metastasis. If the antigen receptor therapy offers an efficacy greater than 50% (see Hypothesis H7 of model (11), then it can be considered a successful treatment against bone metastasis. Even more, a cancer remission is observed and it is possible to recover normal BMU dynamics . This fact can be observed by comparing the blue lines from Fig. 10 with the healthy BMU in the three human life stages from Fig. 1. Thus, the normal BMU dynamics have almost been fully recovered.

5 Conclusions

In this paper, we proposed a bone metastasis model based on the vicious cycle hypothesis and studied the metastatic cancer evolution in three human life stages: childhood, young adult, and adulthood. Next, we posed an optimal control problem from the BM model in order to analyze antigen receptor therapy as a treatment against bone metastasis.
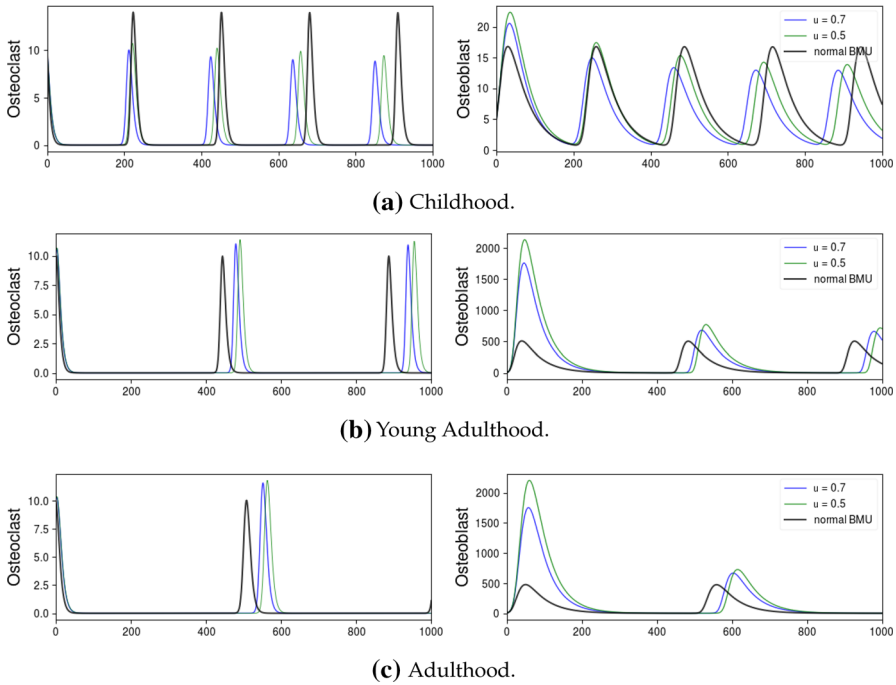
(a) Childhood.

(b) Young Adulthood.

(c) Adulthood.

Fig. 10 Comparison of a normal BMU with the osteoclasts and osteoblasts solution profiles given by the CAR-T cell therapy model under the *Scenario B2* considering effectivities of 50% and 70%

An initial bifurcation analysis was carried out to obtain the parameter values for each human life stage since each stage presents different frequencies and periods of BMU waves. Using qualitative and quantitative analysis of the BM model, we obtained that cancer invasion is much faster when the BMU is more active, which occurs in the childhood stage. In adult patients the cancer invasion is slower, resulting in some cases the invasion failure. We evaluated behaviors of osteoclasts, osteoblasts, cancer cells, and bone mass by considering osteolytic and osteoblastic lesions. We also illustrated cancer oscillation behaviors associated with the pre-metastatic niche hypothesis.

In the second part of our work, the existence of an optimal control solution for the antigen receptor model was proved. Moreover, we explored the use of antigen receptor therapy in two aggressive bone metastasis scenarios. In our study, we investigated the effectiveness required for the antigen receptor binding affinity with cancer cells in order to consider a successful therapy. According to our numerical simulations, if the treatment gives an efficiency percentage greater than 50%, then the treatment is effective. There are human preclinical studies which show an efficacy of 30% in a solid tumor. Here it is important to remark that we are not considering toxicity in our model. Moreover, this therapy breaks the *vicious cycle* between the BMU cells and the cancer cells since over time a normal BMU dynamics is recovered. Thereby, treatment with antigen receptor in the childhood stage would be recommended since in such human life stage bone metastasis is more aggressive.

Currently, experimental techniques are unable to track the local time series dynamics of the bone remodeling cycle and the frequencies of osteoblast and osteoclast oscillations. However, the average trabecular bone area and the number of osteoclasts, osteoblasts, and cancer cells can be obtained through histological examination of mouse models at a given time (Lo et al. 2021; Cook et al. 2016). In mice, the distribution of CAR T cells can also be imaged using fluorescence imaging and tumors can be imaged using bioluminescence imaging, which can be quantified over time to give total tumor burden with and without CAR T cell treatment (Zysk et al. 2017). This type of data can be used to validate global models describing BMU dynamics for a large bone surface such as tibia. For our particular case it is necessary to obtain local data which at the present time is unavailable.

CAR T cells are transforming the management of hematologic malignancies and they have demonstrated promise in cancer therapy. Nevertheless, there are still many hurdles to successfully applying these therapeutic approaches more broadly to solid tumors. However, a growing number of clinical trials have focused on solid tumors, targeting surface proteins, and one of the greatest challenges is the lack of preclinical models to evaluate the safety and efficacy of these complex therapies before human studies or in response to safety issues that are uncovered in early-phase clinical studies. In this sense, our model shows evidence of the efficacy of CAR T cell therapy in the treatment of bone metastasis and provides support to pursue further research into this area. Future mathematical models can be updated to include the pharmacokinetics of CAR-T therapy as well as adverse side effects to the patient.

A Bifurcation analysis

Based on the oscillations frequency, we carried out a bifurcation analysis with the numerical software XPPAUT/AUTO to give parameter values in the childhood, young adults and adulthood. Recalling that the solution of system (1) exhibits limit cycles or stable/unstable oscillations when equation (2) is satisfied. For this analysis, we study the effect of varying the parameters g_{11} and g_{22} on osteoclast steady states (c) in the bone remodeling model.

First, the bifurcation parameter was g_{11} and the other parameters were taken as $g_{22} = 0.0001$, $g_{21} = 1$ and $g_{12} = -0.3$. Figure 11 shows the stability diagram of the equilibrium point and the Hopf bifurcation varying g_{11}. The structure of the bifurcation diagram for model (1) is illustrated in Fig. 11b. Using a two parameter variation we obtained that limit cycles occur when $g_{11} \in [1.099 \quad 1.161048]$ and $g_{22} \in [-0.6104841 \quad 0)$. Recall that negative real-valued for kinetic orders describe inhibition activity. For the second case, the bifurcation parameter was g_{22}. The other parameters were: $g_{11} = 0.90$, $g_{21} = 1$ and $g_{12} = -0.3$ (the smallest/largest allowable values for g_{21} and g_{12} are 0.2 and -0.1 respectively, after that the system does not present oscillations).
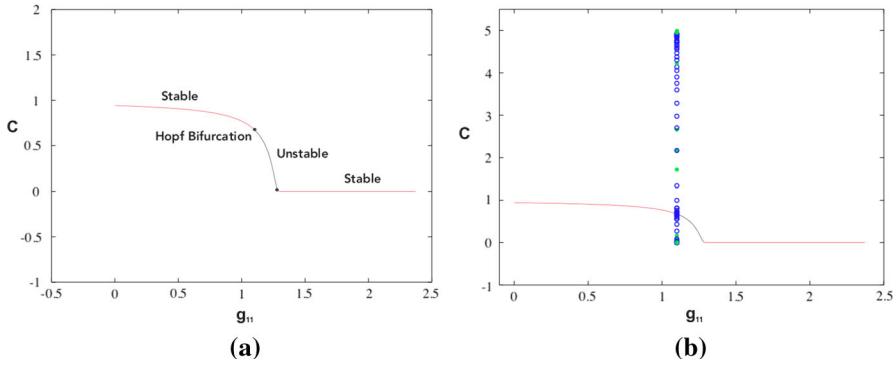
Fig. 11 **a** Stability diagram of the osteoclast, **c** equilibrium point as a function of g_{11}. Red line is stable, and black line is unstable. Hopf bifurcation appears at $g_{11} = 1.1$ and $g_{22} = 0.001$. **b** Bifurcation diagram of the osteoclast, **c** equilibrium for system (1). Green dots represent stable limit cycle and blue circles represent unstable limit cycles (colour figure online)
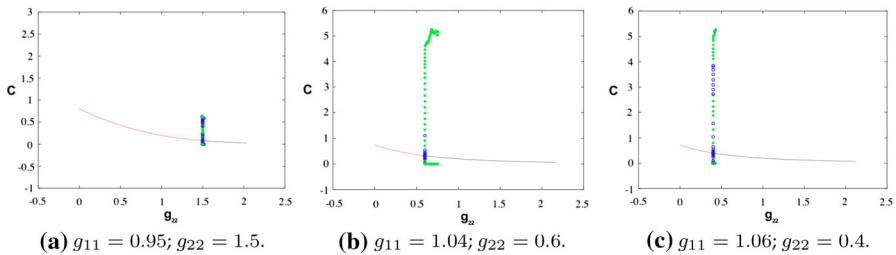

(a) $g_{11} = 0.95; g_{22} = 1.5$.　　**(b)** $g_{11} = 1.04; g_{22} = 0.6$.　　**(c)** $g_{11} = 1.06; g_{22} = 0.4$.

Fig. 12 Hopf bifurcation diagrams of the osteoclast (c) equilibrium point of model (1) as a function of g_{22}. Red line is stable, and black line is unstable. Green dots represent stable limit cycle and blue circles represent unstable limit cycles. Hopf bifurcation occurs at values listed (colour figure online)

Figure 12 shows the diagram of the variation of the equilibrium point and the Hopf bifurcation. Notice that for values of g_{11} less than 0.90 the Hopf bifurcation was not found. Fig. 12a, b show some of the bifurcation dynamics: when parameter g_{22} decreases then the stability region also decreases, and the instability region increases (see red and black lines). In such analysis, we obtained that limit cycles occur when $g_{11} \in [0.90\ \ 1.161]$ and $g_{22} \in [-0.61\ \ 2.0]$, with $g_{12} \in [-1.0\ \ -0.1]$ and $g_{21} \in [0.2\ \ 1.0]$. We also analyzed the oscillations frequency for parameter values close to the bifurcation, which allowed us to classify them in three stage: *(a)* If $g_{12} \in [-0.3\ \ -0.1]$ the BMU is less active, that is BMU has long periods of inactivity (adulthood stage); *(b)* if $g_{12} \in [-0.7\ \ -0.3)$ the BMU is more active, that is, the period of activity is approximately of 6 months (young adult stage), *(c)* finally if $g_{12} \in [-1.0\ \ -0.7)$ the BMU is more active and does not have inactive periods, that is, BMU is constantly remodeling (childhood stage). Therefore, with all the previous information we were able to classify the BMU behavior for three different stages in Table 1.

B Proof of Theorem 3

The existence of optimal solutions for control problem (9)–(12) is obtained if the sufficient conditions of the Filippov-Cesari theorem (Fleming and Rishel 2012) are fulfilled:

(i) The right-hand side of the model (10) is composed of continuous functions, and for each one of these functions f_i there exist positive constant $\mathcal{C}_1$, $\mathcal{C}_2$ such that $| f_i(t, x, u) | \leq \mathcal{C}_1(1+ | x | + | u |)$ and $| f_i(t, \overline{x}, u) - f_i(t, x, u) | \leq \mathcal{C}_2 | \overline{x} - x |$ $(1+ | u |)$ for all $0 \leq t \leq t_f$ and $i = 1, 2, 3$ and $x(t) = (C(t), B(t), T(t))$.

(ii) A solution of the dynamical system (10) is well defined and is unique for an admissible $u \in \Gamma$.

(iii) The set of solutions to system (10) is non-empty and bounded for admissible control functions $u \in \Gamma$.

(iv) The control set Γ is closed, bounded and convex in $\mathbb{R}$.

(v) The right-hand side of the dynamical system (10) is linear in control u.

(vi) The integrand of function (9) is convex with respect to u and satisfies

$$T(t) + \frac{B}{2}u^2(t) \geq \mathcal{K}_1 | u |^\theta - \mathcal{K}_2,$$

with constants $\mathcal{K}_1 > 0, \theta > 1$ and $\mathcal{K}_2$.

Item (i) holds since the model functions are of class C^2 in Ω. Item (ii) holds since the admissible control set Γ contains continuous bounded functions and the right-hand side of (10) is Lipschitz continuous with respect to the three variables C, B and T for admissible $u(t) \in \Gamma$. Using Picard-Lindelöf theorem, there exists a unique solution $(C(t), B(T), T(t)) \in \Omega$ corresponding to the admissible control $u(t) : \mathbb{R}^+ \mapsto [0, u_c]$. When the control variable takes its minimum value, that is, $u(t) = 0$ in (10), we recover the initial model without control (4) whose orbits $C(t)$, $B(t)$ and $T(t)$ of $(C(0), B(0), T(0)) \in \Omega$ are bounded for all $t \geq 0$. Therefore, solutions of the system (10) with $u(t) = 0$ can be regarded as its super-solution. On the other hand, when the control variable is at the upper bound, that is, $u(t) = u_c$, the underlying solution of the system (10) can be regarded as its sub-solutions. Moreover, applying the Carathéodory's existence theorem guarantees the existence of solutions for Cauchy problems. The latter implies that item (iii) holds. Additionally, by the definition of the admissible control set Γ in (12) is clear that this set control is closed, bounded and convex in $\mathbb{R}$. Thus, (iv) holds. To proof the item (v), let $f(t, x, u)$ be the vector function defined by right-hand side of (10), we will find suitable bounds for the states:

$$\begin{aligned} \frac{dC(t)}{dt} &= \alpha_1 C(t)B(t)^{g_{12}} - \beta_1 C(t) + (\sigma_1 - a_1 u(t))C(t)T(t) \\ &\leq C(t)(\alpha_1 m_1 + \sigma_1 C_{max}) \ (g_{12} < 0 \ and \ m_1 := (B_{min})^{g_{12}}). \end{aligned} \quad (18)$$

On the other hand,

$$\frac{dB(t)}{dt} = \alpha_2 C(t)^{g_{21}} B(t) - \beta_2 B(t) + (\sigma_2 - a_2 u(t))B(t)T(t),$$

$$\leq \begin{cases} B(t)(\alpha_2 m_2 + \sigma_2 C_{max}) & if \;\; \sigma_2 \geq 0, \\ B(t)\alpha_2 m_2 & if \;\; \sigma_2 < 0, \end{cases} \tag{19}$$

where $m_2 := (C_{max})^{g_{21}}$. Finally,

$$\frac{dT(t)}{dt} = \alpha_3 C(t)^{g_{31}} T(t)\left(1 - \frac{T(t)}{K}\right) - (\beta_3 + u(t))T(t)$$
$$\leq T(t)(\alpha_3 m_2 - \beta_3). \tag{20}$$

Thus, from (18)–(20) we have that our model is bounded by a linear system. Item *vi)*, the integrand of (9) is quadratic in u, and therefore convex. Condition $T(t) + \frac{B}{2}u^2(t) \geq \mathcal{K}_1 \mid u \mid^\theta -\mathcal{K}_2$ is fulfilled with $\mathcal{K}_2 = 0$, $\theta = 2 > 1$ and $\mathcal{K}_1 = \frac{B}{2} > 0$.

References

Ahmed N, Brawley VS, Hegde M, Robertson C, Ghazi A, Gerken C, Liu E, Dakhova O, Ashoori A, Corder A et al (2015) Human epidermal growth factor receptor 2 (her2)-specific chimeric antigen receptor-modified t cells for the immunotherapy of her2-positive sarcoma. J Clin Oncol 33(15):1688

Araujo A, Cook LM, Lynch CC, Basanta D (2014) An integrated computational model of the bone microenvironment in bone-metastatic prostate cancer. Can Res 74(9):2391–2401

Ayati B, Edwards C, Webb G, Wikswo J (2010) A mathematical model of bone remodeling dynamics for normal bone cell populations and myeloma bone disease. Biol Direct 5(1):28

Bayliss L, Mahoney D, Monk P (2012) Normal bone physiology, remodelling and its hormonal regulation. Surgery (Oxford) 30(2):47–53

Bilezikian JP, Raisz LG, Martin TJ (2008) Principles of bone biology. Academic Press, New York

Bonifant CL, Jackson HJ, Brentjens RJ, Curran KJ (2016) Toxicity and management in car t-cell therapy. Mol Therapy-Oncolyt 3(16):011

Business Wire (2021) U.S. Food and Drug Administration approves Bristol Myers Squibb's and Bluebird Bio's Abecma (idecabtagene vicleucel), the first anti-Bcma car T cell therapy for relapsed or refractory multiple myeloma. https://www.businesswire.com/news/home/20210326005507/en/. Accessed 20 May 2021

Camacho A, Jerez S (2019) Bone metastasis treatment modeling via optimal control. J Math Biol 78(1–2):497–526

Camacho D, Pienta K (2014) A multi-targeted approach to treating bone metastases. Cancer Metastasis Rev 33(2–3):545–553

Cartellieri M, Bachmann M, Feldmann A, Bippes C, Stamova S, Wehner R, Temme A, Schmitz M (2010) Chimeric antigen receptor-engineered t cells for immunotherapy of cancer. J Biomed Biotechnol 2010:956304

Cook L, Araujo A, Pow-Sang J, Budzevich M, Basanta D, Lynch C (2016) Predictive computational modeling to define effective treatment strategies for bone metastatic prostate cancer. Sci Rep 6(29):384

Eladdadi A, Kim P, Mallet D (2014) Mathematical models of tumor-immune system dynamics, vol 107. Springer, Berlin

Eriksen EF (2010) Cellular mechanisms of bone remodeling. Rev Endocr Metab Dis 11(4):219–227

Farhat A, Jiang D, Cui D, Keller ET, Jackson TL (2017) An integrative model of prostate cancer interaction with the bone microenvironment. Math Biosci 294:1–14

Fleming W, Rishel R (2012) Deterministic and stochastic optimal control, vol 1. Springer, Berlin

Garzón-Alvarado DA (2012) A mathematical model for describing the metastasis of cancer in bone tissue. Comput Methods Biomech Biomed Eng 15(4):333–346

Ghaderi S, Lie R, Moster D, Ruud E, Syse A, Wesenberg F, Bjørge T (2012) Cancer in childhood, adolescence, and young adults: a population-based study of changes in risk of cancer death during four decades in norway. Cancer Cause Control 23(8):1297–1305

Gilham DE, Debets R, Pule M, Hawkins RE, Abken H (2012) Car-t cells and solid tumors: tuning t cells to challenge an inveterate foe. Trends Mol Med 18(7):377–384

Gonzalez H, Hagerling C, Werb Z (2018) Roles of the immune system in cancer: from tumor initiation to metastatic progression. Genes Dev 32(19–20):1267–1284

He Q, Liu Z, Liu Z, Lai Y, Zhou X, Weng J (2019) Tcr-like antibodies in cancer immunotherapy. J Hematol Oncol 12(1):99

Heaney RP (2001) Methods in nutrition science: the bone remodeling transient: interpreting interventions involving bone-related nutrients. Nutr Rev 59(10):327–334

Hillerdal V, Essand M (2015) Chimeric antigen receptor-engineered t cells for the treatment of metastatic prostate cancer. BioDrugs 29(2):75–89

Jackson HJ, Rafiq S, Brentjens RJ (2016) Driving car t-cells forward. Nat Rev Clin Oncol 13(6):370

Jerez S, Camacho A (2018) Bone metastasis modeling based on the interactions between the BMU and tumor cells. J Comput Appl Math 330:866–876

Jerez S, Chen B (2015) Stability analysis of a komarova type model for the interactions of osteoblast and osteoclast cells during bone remodeling. Math Biosci 264:29–37

Jilka RL (2003) Biology of the basic multicellular unit and the pathophysiology of osteoporosis. J Comput Appl Math 41(3):182–185

Jinnah AH, Zacks BC, Gwam CU, Kerr BA (2018) Emerging and established models of bone metastasis. Cancers 10(6):176

Juárez P, Guise T (2011) TGF-β in cancer and bone: implications for treatment of bone metastases. Bone 48(1):23–29

June CH, O'Connor RS, Kawalekar OU, Ghassemi S, Milone MC (2018) Car t cell immunotherapy for human cancer. Science 359(6382):1361–1365

Kalos M, Levine BL, Porter DL, Katz S, Grupp SA, Bagg A, June CH (2011) T cells with chimeric antigen receptors have potent antitumor effects and can establish memory in patients with advanced leukemia. Sci Transl Med 3(95):95ra73

Klebanoff C, Yamamoto T, Restifo N (2014) Immunotherapy: treatment of aggressive lymphomas with anti-cd19 car t cells. Nat Rev Clin Oncol 11(12):685–6

Koenders M, Saso R (2016) A mathematical model of cell equilibrium and joint cell formation in multiple myeloma. J Theor Biol 390:73–79

Komarova S, Smith R, Dixon S, Sims S, Wahl L (2003) Mathematical model predicts a critical role for osteoclast autocrine regulation in the control of bone remodeling. Bone 33(2):206–215

Lemos J, Caiado D, Coelho R, Vinga S (2016) Optimal and receding horizon control of tumor growth in myeloma bone disease. Biomed Signal Proces 24:128–134

Lenhart S, Workman J (2007) Optimal control applied to biological models. Chapman and Hall/CRC, Cambridge

Lo CH, Baratchart E, Basanta D, Lynch CC (2021) Computational modeling reveals a key role for polarized myeloid cells in controlling osteoclast activity during bone injury repair. Sci Rep 11(1):1–14

Louis CU, Savoldo B, Dotti G, Pule M, Yvon E, Myers GD, Rossig C, Russell HV, Diouf O, Liu E et al (2011) Antitumor activity and long-term fate of chimeric antigen receptor-positive t cells in patients with neuroblastoma. Blood J Am Soc Hematol 118(23):6050–6056

Lynch CC (2011) Matrix metalloproteinases as master regulators of the vicious cycle of bone metastasis. Bone 48(1):44–53

Ma L, Dichwalkar T, Chang JY, Cossette B, Garafola D, Zhang AQ, Fichter M, Wang C, Liang S, Silva M et al (2019) Enhanced car-t cell activity against solid tumors by vaccine boosting through the chimeric receptor. Science 365(6449):162–168

Manolagas SC (2000) Birth and death of bone cells: basic regulatory mechanisms and implications for the pathogenesis and treatment of osteoporosis. Endocr Rev 21(2):115–137

Mundy G (2002) Metastasis to bone: causes, consequences and therapeutic opportunities. Nat Rev Cancer 2(8):584

Muñoz AI, Tello JI (2017) On a mathematical model of bone marrow metastatic niche. Math Biosci Eng 14(1):289

National Cancer Institute (2021) T cell transfer therapy. https://www.cancer.gov/about-cancer/treatment/types/immunotherapy/t-cell-transfer-therapy

Neilan RM, Lenhart S (2010) An introduction to optimal control with an application in disease modeling. In: Modeling paradigms and analysis of disease trasmission models, pp 67–81

Newick K, Moon E, Albelda S (2016) Chimeric antigen receptor t-cell therapy for solid tumors. Mol Ther Oncolyt 3(16):006

Ottewell PD (2016) The role of osteoblasts in bone metastasis. J Bone Oncol 5(3):124–127

Paget S (1889) The distribution of secondary growths in cancer of the breast. Lancet 133:571–573

Parfitt AM (1994) Osteonal and hemi-osteonal remodeling: the spatial and temporal framework for signal traffic in adult human bone. J Cell Biochem 55(3):273–286

Porter DL, Levine BL, Kalos M, Bagg A, June CH (2011) Chimeric antigen receptor-modified t cells in chronic lymphoid leukemia. N Engl J Med 365:725–733

Randall R, Lewis V, Weber K (2016) Metastatic bone disease. An integrated approach to patient care. Springer, New York

Rhodes A, Hillen T (2019) A mathematical model for the immune-mediated theory of metastasis. J Theor Biol 482(109):999

Rhodes A, Hillen T (2020) Implications of immune-mediated metastatic growth on metastatic dormancy, blow-up, early detection, and treatment. J Math Biol 81(3):799–843

Rosenberg S (2011) Cell transfer immunotherapy for metastatic solid cancer-what clinicians need to know. Nat Rev Clin Oncol 8(10):577

Ryser M, Komarova S, Nigam N (2010) The cellular dynamics of bone remodeling: a mathematical model. SIAM J Appl Math 70(6):1899–1921

Sarkar RR, Gloude NJ, Schiff D, Murphy JD (2019) Cost-effectiveness of chimeric antigen receptor t-cell therapy in pediatric relapsed/refractory b-cell acute lymphoblastic leukemia. JNCI J Natl Cancer Inst 111(7):719–726

Savageau MA (1988) Introduction to S-systems and the underlying power-law formalism. Math Comput Model 11:546–551

Sousa S, Clézardin P (2018) Bone-targeted therapies in cancer-induced bone disease. Calcif Tissue Int 102(2):227–250

US Food and Drug Administration (2021) Package insert—abecma. https://www.fda.gov/media/147055/download. Accessed 20 May 2021

Vera J, Balsa-Canto E, Wellstead P, Banga JR, Wolkenhauer O (2007) Power-law models of signal transduction pathways. Cell Signal 19(7):1531–1541

Voit E (1991) Canonical nonlinear modeling: S-systems approach to understanding complexity. Chapman & Hall, Cambridge

Walsh JS (2015) Normal bone physiology, remodelling and its hormonal regulation. Surgery (Oxford) 33(1):1–6

Wang RA, Li QL, Li ZS, Zheng PJ, Zhang HZ, Huang XF, Chi SM, Yang AG, Cui R (2013) Apoptosis drives cancer cells proliferate and metastasize. J Cell Mol Med 17(1):205–211

Weiner M, Weiner SL, Simone JV (2003) Childhood Cancer Survivorship: Improving Care and Quality of Life. Institute of Medicine (US) and National Research Council (US) National Cancer Policy Board. National Academies Press (US)

Wiggers SL, Pedersen P (2018) Routh-hurwitz-liénard-chipart criteria. Structural stability and vibration. Springer, Cham, pp 133–140

Zhao L, Cao Y (2019) Engineered t cell therapy for cancer in the clinic. Front Immunol 10:2250

Zumsande M, Stiefs D, Siegmund S, Gross T (2011) General analysis of mathematical models for bone remodeling. Bone 48(4):910–917

Zysk A, DeNichilo MO, Panagopoulos V, Zinonos I, Liapis V, Hay S, Ingman W, Ponomarev V, Atkins G, Findlay D et al (2017) Adoptive transfer of ex vivo expanded vγ9vδ2 t cells in combination with zoledronic acid inhibits cancer growth and limits osteolysis in a murine model of osteolytic breast cancer. Cancer Lett 386:141–150